J Mol Model (2003) 9:348–354
DOI 10.1007/s00894-003-0158-5

ORIGINAL PAPER

Sergio Manzetti

Computer modeling and nanosecond simulation of the enzyme–substrate complex of the common lymphoblastic leukemia antigen (neprilysin) indicates shared residues at the primary specificity pocket (S1') with matrix metalloproteases

Received: 17 April 2003 / Accepted: 11 July 2003 / Published online: 29 August 2003

Abstract The common acute lymphoblastic leukemia antigen (neprilysin, CD10, neutral endopeptidase 24.11) is a member of the neprilysin family, and projects functions in signaling pathways in pathophysiological processes such as cancer, Alzheimer's disease and hypertension. Given its pathophysiological importance, an investigation of the natural substrate specificity of this metalloprotease is presented here through the application of enzyme–substrate modeling and molecular dynamics simulations. The results show that the substrate modeled, LATAC↓FG, satisfies a complementary backbone H-bonding with Ala543–Tyr545, thereby suggested to be the putative substrate-binding beta-sheet, analogously to matrix metalloproteases. The modeling further suggests that phenylalanine at the P1' position (substrate) is directed in the same fashion as the synthetic inhibitor of the reference crystal structure and that this enzyme does not bind the P3'/P4' positions of a substrate, as other metalloproteases do. After a specific comparison with one member of the matrix metalloproteases, MMP-3, a common conserved valine residue at the primary S1' subsite was found to be shared between these two otherwise different proteases. These results may prove useful for selective drug design for neprilysin, and lay a foundation for future subsite analysis for other members of the neprilysin family.

Keywords Cancer · Neprilysin · Modeling · Simulation · Substrate · Specificity

Electronic Supplementary Material Supplementary material is available for this article if you access the article at http://dx.doi.org/10.1007/s00894-003-0158-5. A link in the frame on the left on that page takes you directly to the supplementary material.

S. Manzetti (✉)
Proinformatix.com,
Lippestad, 1825 Tomter, Norway
e-mail: Sergio@proinformatix.com
Tel.: +47 4547-4913

Introduction

The neprilysin superfamily is a group of zinc-endopeptidases involved in pathophysiological processes such as Alzheimer's disease, cancer, hypertension, asthma, cerebral vasospasm and congestive heart failure through their central role in the hydrolysis and activation of bioactive peptides such as bradykinin, endothelin, enkephalin, tachykinin, substance P and neurotensin [1, 2, 3, 4, 5, 6]. The best known members of the neprilysins are the common acute lymphoblastic leukemia antigen (neprilysin, neutral endopeptidase 24.11), the Kell blood-group protein, the phosphate regulating gene with homologies to endopeptidases on the X chromosome (hypophosphatemia, vitamin D resistant rickets), ECE 1&2[1], X-converting enzyme and NL1 that share a local homology of 25% to 50%. [7, 8, 9, 10, 11, 12, 13] The neprilysins assemble a globular membrane-bound ectodomain exposed to the extracellular matrix. [11, 14, 15].

The understanding of the functional and physiological roles of the various members of the neprilysins, as for any novel protein, relies on extended studies on their activity towards physiological and chromogenic substrates, their expression patterns, their cellular localization and notably, the chemical composition of their special substrate-binding clefts, which determines the affinity toward distinct substrates. The primary specificity pocket (S1') of some neprilysins especially for NEP[2], has recently been investigated using site-directed mutagenesis, synthetic inhibitors and crystallographic data. [11, 16, 17, 18]. However, although more knowledge is gradually being gained around its primary specificity site (S1'), no empirical or computational knowledge is available about the dynamic and chemical properties of this subsite, neither the second subsite, S2', and the S-region *when* interacting with natural peptide sidechains. Not to mention, the entire natural binding-modus of an oligopeptide

[1] Endothelin converting enzyme.
[2] Neprilysin 24.11.

to a neprilysin is unknown, given the lack of crystallized complexes of one of these enzymes with natural inhibitors (as crystallized for MMP-3[3] [19]) or with a trapped natural substrate, as accomplished for serine proteases. [20]

The knowledge of how the natural substrate binds to the enzyme is fundamental to design better and more specific drugs. The use of computer modeling to construct enzyme–substrate models has recently been applied [21] and gave coherent results with the present knowledge of substrate affinity and binding for a group of metzincins. [19, 22] Previous modeling approaches of the apoenzymes of two neprilysins (ECE and NEP) have been published; [23, 24, 25] however, no enzyme–substrate complex was supplied and investigation of this possible interface is still not hypothesized.

Using the only neprilysin crystallized to date (neprilysin [11]), the scope of this project is to construct an enzyme–substrate model for this structure, based on the similarity hereby observed at the active site to a matrix metalloprotease, the MMP-3/TIMP-1[4] crystal structure. MMP-3 (stromeolysin-1) is a metzincin that is involved in pathophysiological processes such as tissue remodeling and extracellular matrix degradation, [26] while TIMP-1 is its natural inhibitor that resembles a cleaved substrate at the binding interface. [19] These two otherwise different enzymes do, as we shall see, share very similar binding pockets. The results based on this observation do in the opinion of the author, supply novel data that may aid in developing a deeper understanding on how neprilysins bind their substrates and which subsites determine the affinity. The supplied enzyme–substrate model of NEP will also aid in determining the subsites for other neprilysins, with the use of comparative modeling, and computer simulations.

Materials and methods

Enzyme–substrate modeling

All modeling approaches were carried out using SWISS PDB Viewer. [27] The model of NEP in complex with a hypothetical substrate was built using the structure of MMP-3 in complex with TIMP-1 (1UEA) as template. Because these two structures have virtually no common overall fold, the common catalytic center (His^1–Zinc–His^2 and Glu^{cat}) was used as superimposition target. The superimposition of all atoms for the four residues at the catalytic center yielded a RMSD[5] of 0.4 Å, which suggests this as the ideal superimposition target between zinc-endopeptidases. Cys1 and Thr2 from TIMP-1, which binds in a similar fashion as the P' segment of a cleaved substrate, [19, 22] were merged to a common layer with NEP. The structural extrapolation gave the reproduction of the conserved H-bonds as found in MMP-3 and TIMP-1. However, a delicate manual adjustment was performed on the resulting P' dipeptide (see next paragraph) in order to mimic accurately the native H bond network and the localization of the N terminus to the catalytic zinc ion (which indicates the approximate positions of the scissile bond), as occurred in the crystallized complex of MMP-3/TIMP-1.

The experimental P-region was built by adding five residues in an H-bonded antiparallel beta-sheet manner as the P' region. These residues were constructed from the N-terminal Cys1 residue, creating the elongated substrate spanning P5–P2'.

The composition of P1–P1'–P2' was chosen on the basis of kinetic data supplied by Watanabe et al., [28] while the composition of P5-P2 was determined based on the methodology of fitting residues complementary to a surface [29, 30] resulting in a substrate with the following sequence; LATAC↓FG. The substrate was at this stage minimized preliminarily in vacuo to the rigid crystal structure using 50 steps of steepest descent method, and subsequently analyzed for free energies of binding with the program STC. [31]

Molecular dynamics preparation and simulation

The nanosecond simulation of NEP and substrate was prepared in a virtual box of 730 nm^3 (vector units 9×9×9) filled with 20,639 water molecules encompassing a system of 73,060 atoms. All N/C termini were assigned the neutral state and the histidine residues were protonated at their delta nitrogen. The neutral termini were chosen because the system was not neutralized, so to avoid interference of neutralizing ions at the zinc–substrate interface. Flexible water molecules [32] were adapted to the enzyme–substrate complex with 500 steps of energy minimization (steepest descent). The enzyme was immobilized (in the input parameter file) so the flexible waters could adjust to its empirical state, while the substrate was not immobilized and adjustable with the enzyme and solvent according to chemical and geometrical satisfaction. The simulation was performed using the GROMACS 3.1.4 package [33] with the OPLS-AA/L force field. [34] The SPC water model (single point charge [35]) was used to simulate the solvent phase, and an integration step size of 2 fs was applied. Electrostatics were simulated with a Generalized Reaction Field [36] (GRF) with a Coulomb cut-off of 9 Å and a Lennard-Jones cut-off of 15 Å (in the author's personal experience, these cut-offs have shown to be appropriate for large systems when using GRF). Temperature coupling was set to 298 K and the pressure was kept at 1 atm using the Berendsen temperature- and pressure-coupling scheme. [37] H bonds were simulated using the LINCS algorithm, [38] and all other bonds were simulated using a harmonic potential. The two histidine residues (HEXXH motif) and the catalytic zinc ion they chelate were kept immobilized during the simulation, because these residues are struc-

[3] Matrix metalloprotease 3.
[4] Tissue Inhibitor for MetalloProtease.
[5] Root-mean-square-deviation.

turally stable at ground/transition state. [39] In this way, the position of the substrate and surrounding residues would adapt to the rigid catalytic center, which has previously shown to become victim to artifacts easily because of an imperfect topology for the special catalytic zinc ion (David van der Spoel, personal communication).

Trajectory and molecular analysis

Analysis of the trajectory was carried out with the programs, g_rms, g_mdmat, g_trajconv and xpm2ps, incorporated in the GROMACS package. RMSD graphs were produced using the program XmGrace 5.1.8 (Wis Plasma Laboratory, Weizmann institute of Science, Israel, http://plasma-gate.weizmann.ac.il/Grace/). SWISS PDB Viewer [27] was used for visual analysis and graphical representation, VMD [40] for animation and FRED incorporated in VIDA (Open Eye Scientific software, Santa Fe, NM 87507, www.eyesopen.com) to estimate the hosting potential of the binding pockets.

Results and discussion

Common binding clefts between MMPs and neprilysins

In order to study the binding site of NEP a structural comparison was done with the well-characterized binding site of MMP-3, a matrix metalloprotease part of the metzincin superfamily. This comparison was based on a structural superimposition with the zinc centers as target.

The superimposition shows that NEP and MMP-3 indeed share very similar binding sites (Fig. 1). A typical antiparallel substrate-binding beta-sheet found in MMP-3 (as in all metzincins), [19, 22] is also found in NEP, and is located between Ala543–Ser547. On the opposite side of the binding cleft of metzincins, a short parallel beta-anchor binds the P2'–P3' portion of the substrate. [22] This segment was not found in NEP, something that can correlate with its carboxypeptidase and endopeptidase-activity. [1]

Indeed, when compared to MMP3, NEP shows limited hosting space in terms of "length" at the S' side of the binding pocket (see Fig. 1). In fact, the S' side of neprilysins is confined by a group of aromatic residues (Phe106, Phe563, and Trp693) which creates an interrupting "wall" on the P' side of the catalytic zinc ion, limiting the length of the S' region (see Fig. 1). Öfner and colleagues (2000) [11] defined the S1' pocket by Phe106, Ile558, Phe563, Met579, Val580, Val692 and Trp693 based on the interaction with the co-crystallized phosphoramidon inhibitor. Considering the iterative superimposition of the two binding clefts, three key residues of the well-characterized S1' subsite from MMPs (Leu164, Val198 and Pro221) are directly superimposable with three of the reported residues, Ile558, Val580 and Arg717 (see Fig. 1). The central specificity determinant in MMP-3, which is also present in other MMPs, is Val198, [41, 42, 43] thereby projecting conserved characteristics between the S1' pockets of MMPs and of NEP.

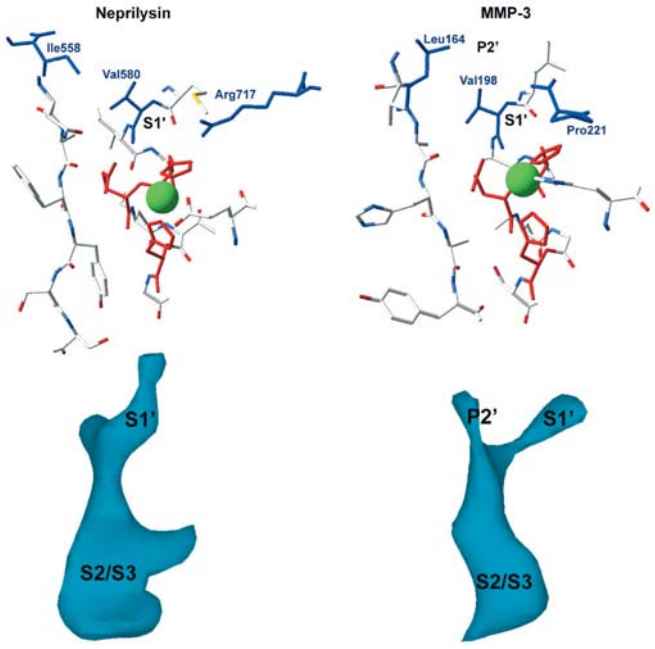

Fig. 1 A representation of the binding pockets of NEP and MMP-3. *Top row:* NEP (*top, left*) shows a conserved set of primary specificity determinants (*blue*) supplying similar chemical qualities toMMP-3 (*top, right*) to bind the substrate. Arg717 showed in the molecular dynamics simulations to establish a salt bridge with the carboxy terminus from the substrate, and to neutralize its excessive charge in the binding pocket (in accord with in vitro confirmed carboxypeptidase activity of neprilysin. [44] *Bottom row:* the volume of these pockets is shown colored by depth, which indicates an end in binding at P1'/P2' for NEP (*bottom, left*), compared to MMP-3 which has a binding interface to the host P2'–P3'–P4' residues (*bottom, right*). [19] The S2/S3 regions show a big difference between NEP and MMP-3, which most conceivably prefers bulkier residues

An S2' subsite was suggested by Öfner and colleagues [11] to be confined by Arg102, Asp107, and Arg110; however, in the comparison with MMP-3, three residues from NEP, Phe106, 563 and Trp693, are perpendicularly inclined and block the further running of the substrate in an extended conformation. NEP cleaves short oligopeptides and it has also exerted carboxypeptidase activity, [44] which may therefore suggest that a P2' is superfluous for an ideal substrate, given the presence of these "blocking" residues (see the void binding volume of pockets, Fig. 1).

Enzyme–substrate model

The enzyme–substrate model for NEP was built on the basis of the structural superimposition with MMP-3. The N-terminal segment from the MMP-3 inhibitor (TIMP-1), which is similar to the P'-region of a substrate, [19] was reproduced in complex with NEP. This segment fitted geometrically well in the cleft of NEP. However, the P3' and P4' residues clashed directly with the "aromatic wall"

mentioned above. The P3' and P4' residues were for that reason removed.

In order to build the P region (opposite side to scissile bond), which is less known for zinc proteases, four experimental and computational fitting residues were added to the cysteine residue in favorable extended beta-sheet conformation (see methods). The importance of the extended conformation at the P' and P regions of a substrate of proteases has been elucidated, [45, 46] and is therefore along with the details of the MMP-3/TIMP-1 binding site, the cornerstone of this modeling approach.

After the model was built, the backbone H bonding on the P' side was represented by two H bonds between both backbone atoms of Phe (P1') and the complementary backbone atoms from Ala543 on the enzyme (Fig. 2a). On the opposite side of the scissile bind (P side), Ala at the P2 position was H bonded via the backbone atoms to Tyr545, in addition to sidechain-to-backbone H bonds between Thr (P3) and Ser547 (see Fig. 2).

The plausibility of the constructed enzyme–substrate model is primary strengthened by the satisfaction of the backbone H bond donors from Ala543–Tyr545 (which are located at the same positions as their MMP counterparts, see Fig. 1), secondary by sidechain-to-backbone H bonds between P3 and Ser547 (increases stability at the P region) and tertiary by molecular complementarity (see Fig. 3). The theoretical free energy of binding of the substrate (total: -6.9 kJ mol^{-1}) showed that the chosen residues are well associated with the enzyme surface, as modeled in antiparallel beta-sheet conformation with the enzyme. Phenylalanine at P1', which has the lowest theoretical free energy of binding, interacts with the hydrophobic sidechains of Val580 and Ile558, in an analogous manner with the leucyl moiety of the phosphoramidon inhibitor. [11] The P2' residue has its carboxyl group close to Phe106, a position that, according to empirical [47] and force field data (see methods), is unfavorable because a carboxyl inclination towards π electrons (Phe106) is repulsive, and the only "way out" for this C terminal from the P2 residue would be an illegal Phi/Psi of 120/60. In order to investigate for better fit at this position, a glycine was inserted at P2' to allow more torsional flexibility in the molecular simulations.

After this position, it appears that there is no more space to accommodate another residue in the beta-sheet extended P' direction, (as occurs in MMPs and ADAMs up to the P4'/P5' positions [19, 48]). However, on the opposite side of the zinc ion/"scissile bond", the enzyme has a rather wider and longer space for accommodating beta-sheet extended residues (see Fig. 1) towards a putative S4/S5 pocket defined by Pro295, Tyr346 and Leu298 and Phe596, which hosted an alanine residue at the P4 position and a leucine at P5, still in a favorable extended beta-sheet conformation during the substrate-building procedure (Fig. 2).

Using molecular dynamics over a nanosecond interval the dynamics of the enzyme–substrate interface is assessed, and the interacting substrate-specific sidechains are attempted identified in a solvated dynamic system.

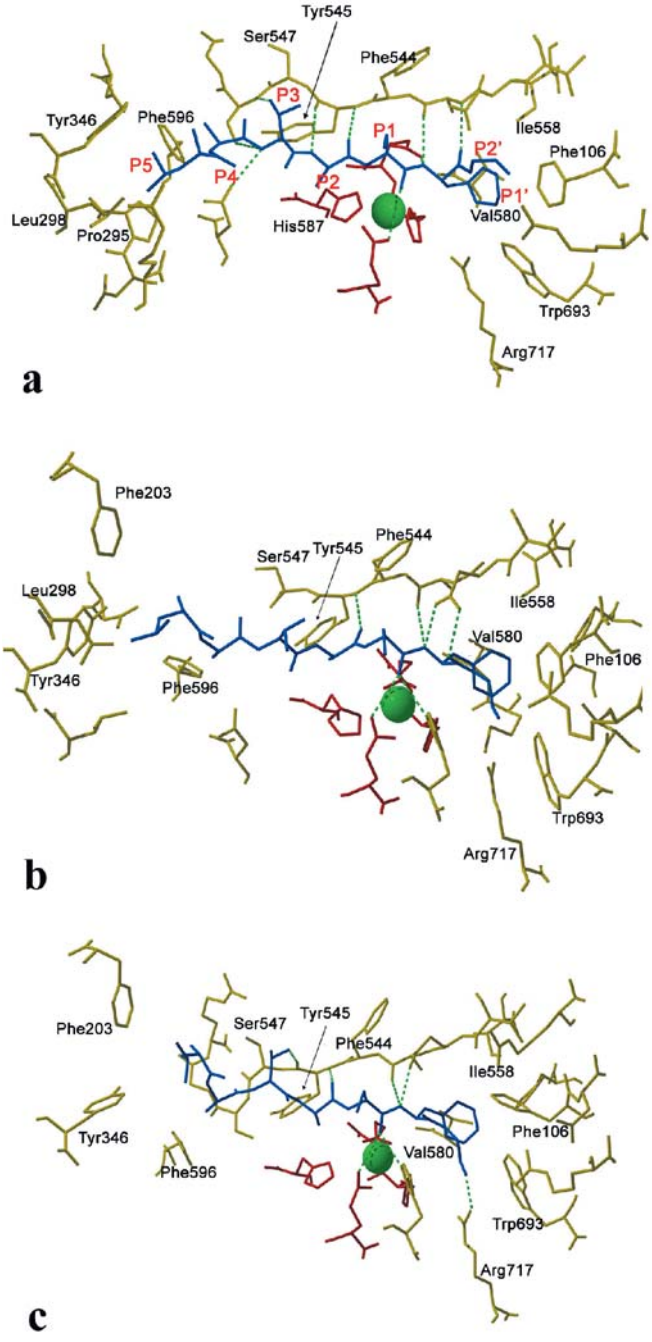

Fig. 2a–c A schematic illustration of the three central stages during the computer modeling study: **a** the binding site with substrate before simulation (0 ps) (see also Fig. 3); **b** the binding site at 500 ps; **c** the binding site at the end of the simulation, 1,000 ps. Some residues are not shown for graphical purposes. For graphical purposes only H bonds are represented by *green* lines, all other interactions are reported in Table 1

Molecular simulations

Given the size of the system (73,060 atoms), financial and practical limitations, the simulation was carried out for only 1 ns, which can be too short to identify certain weaknesses in the enzyme–substrate model. In order to

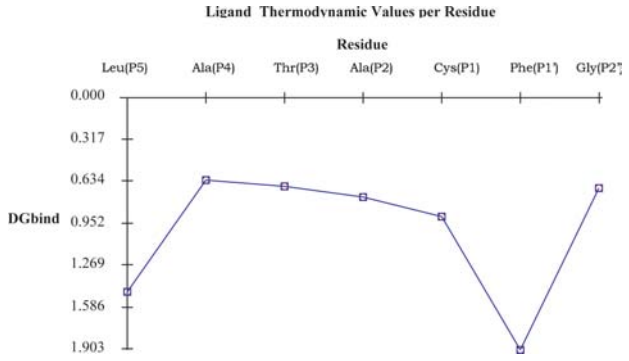

Fig. 3 Graphical representation of the computed binding energies of the modeled substrate in complex with the crystal structure of NEP. Free energy of binding (*y*-axis) for each residue (*x*-axis) is reported in kJ mol^{-1}, calculated using the program STC. [31]

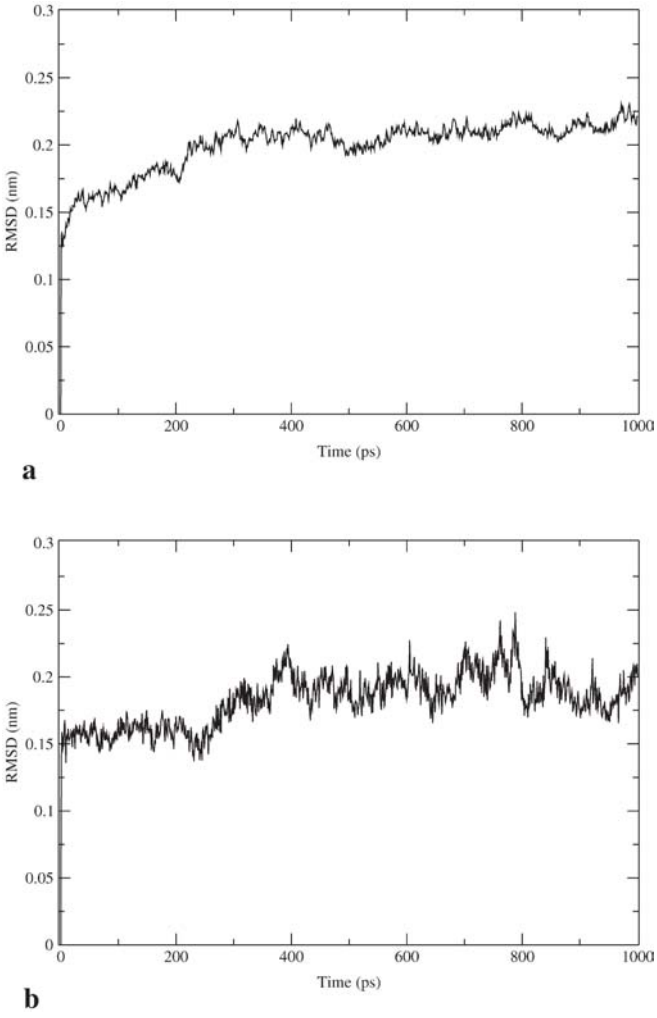

Fig. 4a–b Structural monitoring of the enzyme–substrate system. **a** RMSD fluctuations of the enzyme. **b** RMSD fluctuations of the substrate

comply with this, a thorough analysis of the binding site is described below, and the strongest deviations are pointed out. The analysis of the interactions at the interface (contact maps and visual inspection Fig. 2 and Table 1) were deduced from the most stable interval of the substrate, between 400 and 600 ps (deviation of C-alpha by RMSD to the input conformation, see Fig. 4a, b). The changes that occurred in the substrate are, as we shall see, mostly located in the terminal segments, and are discussed thoroughly below.

The putative S'/P' side

The S' region is centrally stabilized by the hydrophobic lock of the S1' pocket plus a backbone H bond between Ala543 and P1', while the second H bond with the carbonyl group of P1' alternatively shifted from interacting with Ala543 and the sidechain of Asn542. The sidechain of phenylalanine at P1' interacted with Met579, Val580, Trp693, Phe563 and Ile558, where Val580 was central in the interaction. At the beginning of the simulation the closest sidechains to the phenyl moiety of Phe (P1') were Val580, Trp693 and Ile558, at

Table 1 A list of the interacting residues as identified using contact maps (computed in the interval 400–600 ps—see Fig. 4), and visual inspection of the three central stages (0 ps, 500 ps, 1,000 ps—Fig. 2) of the computer analysis of NEP in complex with a hypothetical substrate

Substrate residue	Enzyme subsites	Interaction
P2'-Gly	Phe106, Arg717	Gly(C-term) ionic to Arg717(Gu) Gly(H) to Phe106(Ph)
P1'-Phe	Val580, Ile558, Trp693	Phe(CZ) aromatic to Trp693(Ch2,CZ3) Phe(Ph) hydrophobic to Val580(Cβ, Cγ1,2) Phe(Cε2) hydrophobic to Ile558(Cδ1)
P1-Cys	Solv, Phe544	Cys(Cβ) hydrophobic to Phe(Cβ)
P2-Ala	Tyr545, His587	Ala(C, N) H-bond to Tyr 545 (C, N) Ala(Cβ) hydrophobic to His587(Cγ)
P3-Thr	Solv, Ser547	Thr(Oγ) H-bond to Ser547(Oγ) & Solv.
P4-Ala	Phe596	Ala Cβ) hydrophobic to Phe596(Ph)
P5-Leu	Pro295, Tyr346, Leu298, Phe203	Leu(Cδ1,2) hydrophobic to Phe203(CZ) Leu(Cδ1,2) hydrophobic to Leu298(Cβ,δ1) Leu(Cδ2) hydrophobic Tyr346(Ph) Leu(Cδ2,β) hydrophobic to Pro295(Cβ, γ)

500 ps Val580 and Ile558 remained at the status quo while Met579 approached closer with the distancing of Trp693. At 1,000 ps the sidechain of Met579 drifted away from its weak interaction with Phe (P1') in addition to Trp693, while Val580 remained stable and Ile558 went from a *cis* to a *trans* conformation, still in the same position.

The stability of the sidechains in the pocket describes qualities of binding in a solvated and associated dynamic situation. The firm stability of Val580 and Ile558 suggests that these residues may play a bigger role in binding the P1' sidechain and that they are less influenced by the solvent, that they function as the central determinants in the hydrophobic lock with the presented lock and key mechanism. In order to support this theory, and in respect to the excellent work performed by Öfner et al. (2000), [11] a comparison with empirical data is carried out. The empirical results by Öfner and colleagues show that the leucyl moiety of the phosphoramidon inhibitor is inclined towards Val580, identically as the sidechain of the P1' phenylalanine sidechain is as seen at 0 ps, 500 ps and 1 ns. This indicates indeed a high accord between the computational results with a "natural" peptide and the synthetic inhibitor mimics the natural peptide sidechain. However, a more striking feature was observed when these residues were compared to the equivalent pocket of MMP-3. [19] The inclination of the threonine sidechain from the TIMP-1 inhibitor (P1') in complex with MMP-3 is virtually identical to the inclination of the leucyl moiety from the phosporamidon inhibitor in the crystal structure, [11] and of the phenylalanine sidechain from the enzyme–substrate model. By relevance, the central residues in the pocket of MMP-3 are Leu164 and Val198, [41, 42] which shows a strong chemical familiarity with the equivalent residues in NEP (Ile558 and Val580) pockets (see Figs. 1 and 2). For this reason, it is conceivable to presume that S1' inhibitors and even clinically applied drugs from matrix metalloproteases may have an interfering inhibition on neprilysins.

Moving to the end of the P' region, the P2' sidechain was inclined towards a gap between the two sidechains of Phe106 and Trp693 at 0 ps, in a similar orientation as the indole moiety of the phosphoramidon inhibitor. [11] Throughout the simulation, this inclination of Gly(P2') changed to interact with Arg717 and Phe106.

In this context, the guanidinium group from Arg717 has its position equivalent to the carbon ring of Pro221 from MMP-3 (Fig. 1). The role of Pro221 in MMPs is to confine the S1' pocket and to supply it backbone in substrate binding. [41, 42] Interestingly, the carboxypeptidase activity reported for NEP [43] correlates well with the hypothesis of that Arg717 would easily neutralize the C-terminal charges of the P1' residue oriented in this direction.

The putative S/P side

The sidechain of the catalytic glutamate from the enzyme, moved into coordination with the zinc ion, as also previously observed with ADAM[6]s and MMPs, [21] and the histidine residues moved slightly back from the zinc ion, although they were frozen, which is an artifact of the simulation. Cysteine at P1 remained in a stable contact with the solvent, directing its hydrophobic moiety towards Phe544, one of the central residues of the antiparallel substrate-binding beta-sheet. Further down the substrate, the sidechain of alanine at P2 was in a hydrophobic contact with the C_β of Tyr545, and remained well H-bonded to it as well through its backbone atoms. Threonine at P3 contributed its sidechain in a continuous competition with the backbone carbonyl of P4 in establishing an H-bond with Ser547. This H-bond was the second anchor on the P-side of the scissile bond, and was at the same time the last anchor for stability on the P-side. This is explained by the fluctuations of the P5 residue, which moved 6.2 Å from its original position. These fluctuations indicate one of the following (a) this region of the substrate is incompatible with the enzyme or (b) the hydrophobic attraction to the S4/S5 cleft is not sufficient to lock this position in place and requires additional backbone H bonds. In the first case, the incompatibility is not strong given that the residues Pro295, Tyr346 and Leu298 supply a satisfying hydrophobicity to host the Leucine sidechain at P5 and in fact yield the next-most optimal free energy of binding (~ −1.3 kJ mol^{-1}) of the entire substrate (Fig. 3). The latter is most likely the explanation, because other residues that were H bonded in the simulation were far more stable (Fig. 2). In other words, the S5/P5 position either has no or a small role in binding, and the enzyme does not seem to require it for specific substrate binding and recognition.

Conclusion

Revealing a conserved binding pocket to MMPs, the common acute lymphoblastic leukemia antigen putatively binds the substrate in an extended beta-sheet conformation, which centrally satisfies four H bonds donated by two residues from the substrate-binding beta-sheet on the enzyme, Ala543–Tyr545. NEP and MMP-3 share also two quite similar S1' cavities, with Ile558 and Val580 and Leu164 and Val198 as central determinants for specificity. This feature, indicates an opportunity in applying conventional S1' pocket inhibitors designed for matrix metalloproteases in in vitro experiments directed at neprilysins. At the same time, this homology indicates also a risk of toxicity for clinical inhibitors, which might interfere in vivo with vital signaling pathways of NEP. As found from the computer modeling in this study, NEP binds a substrate preferably between P4 and P1', and designates a general hydrophobic specificity. These

[6] A disintegrin and metalloprotease domain.

results give a broader basis to identify and target new areas in the binding site of NEP, and other neprilysin members, and hopefully more studies directed to cross-inhibition of neprilysins and MMPs.

Supplementary material

An animation of a short interval of the simulation is available as supplementary material and has also been posted on the World Wide Web, at http://www.proinformatix.com/nep.html. PDB coordinates have been posted at the PDB databank under the identity 1MB7.

Acknowledgements I would like to thank Anthony Nicholls from Openeye Scientific Software for lending the software package VIDA for this project, GlaxoSmithWellcome, Gromacs.org, the Weizmann institute of Science and the Sykes group for publishing their software freely on the web.

References

1. Carson JA, Turner AJ (2002) J Neurochem 81:1–8 (Review)
2. Papandreou CN, Usmani B, Geng Y, Bogenrieder T, Freeman R, Wilk S, Finstad CL, Reuter VE, Powell CT, Scheinberg D, Magill C, Scher HI, Albino AP, Nanus DM (1998) Nat Med 4:50–57
3. Wallace EM, Moliterni JA, Moskal MA, Neubert AD, Marcopulos N, Stamford LB, Trapani AJ, Savage P, Chou M, Jeng AY (1998) J Med Chem 41:1513–1523
4. Hoang MV, Turner AJ (1997) Biochem J 327:23–26
5. Johnson GD, Stevenson T, Ahn K (1999) J Biol Chem 274:4053-4058
6. Matsas R, Kenny AJ, Turner AJ (1984) Biochem J 223:433–440
7. Shipp MA, Richardson NE, Sayre PH, Brown NR, Masteller EL, Clayton LK, Ritz J, Reinherz EL (1988) Proc Natl Acad Sci USA 85:4819–4823
8. Lee S, Zambas ED, Marsh WL, Redman CM (1991) Proc Natl Acad Sci USA 88:6353–6357
9. Francis F, Strom TM, Hennig S, Boddrich A, Lorenz B, Brandau O, Mohnike KL, Cagnoli M, Steffens C, Klages S, Borzym K, Pohl T, Oudet C, Econs MJ, Rowe PS, Reinhardt R, Meitinger T, Lehrach H (1997) Genome Res 7:573–785
10. Xu D, Emoto N, Giaid A, Slaughter C, Kaw S, deWit D, Yanagisawa M (1994) Cell 78:473-485
11. Öfner C, D'Arcy A, Hennig M, Winkler FK, Dale GE (2000) J Mol Biol 296:341–349
12. Ghaddar G, Ruchon AF, Carpentier M, Marcinkiewicz M, Seidah NG, Crine P, Desgroseillers L, Boileau G (2000) Biochem J 347:419–429
13. Valdenaire O, Richards JG, Faull RL, Schweizer A (1999) Brain Res Mol Brain Res 64:211-221
14. Kerr MA, Kenny AJ (1974) Biochem J 137:477–488
15. Erdos EG, Skidgel RA (1989) FASEB J 3:145–151
16. Marie-Claire C, Tiraboschi G, Ruffet E, Inguimbert N, Fournie-Zaluski MC, Roques BP (2000) Proteins 39:365–371
17. Chen H, Noble F, Coric P, Fournie-Zaluski MC, Roques BP (1998) Proc Natl Acad Sci USA 95:12028–12033
18. Inguimbert N, Coric P, Poras H, Meudal H, Teffot F, Fournie-Zaluski MC, Roques BP (2002) J Med Chem 45:1477–1486
19. Gomis-Rüth FX, Maskos K, Betz M, Bergner A, Huber R, Suzuki K, Yoshida N, Nagase H, Brew K, Bourenkov GP, Bartunik H, Bode W (1997) Nature 389:77–81
20. Wilmouth RC, Edman K, Neutze R, Wright PA, Clifton IJ, Schneider TR, Schofield CJ, Hajdu J (2001) Nat Struct Biol 8:689–694
21. Manzetti S, McCulloch DR, Herington AC, van der Spoel D (2003) J Comput Aided Mol Des (in press)
22. Johnson LL, Pavlovsky AG, Johnson AR, Janowicz JA, Man CF, Ortwine DF, Purchase II CF, White AD, Hupe DJ (2000) J Biol Chem 275:11026–11033
23. Bur D, Dale GE, Oefner C (2001) Protein Eng 14:337–341
24. Sansom CE, Hoang MV, Turner AJ (1998) Protein Eng 11:1235–1241
25. Tiraboschi G, Jullian N, Thery V, Antonczak S, Fournie-Zaluski MC, Roques BP (1999) Protein Eng 12:141–149
26. Nagase H (1996) In: Hooper NM (ed) Zinc metalloproteases in health and disease. Taylor and Francis, London, pp 153–204
27. Guex N, Peitsch MC (1997) Electrophoresis 18:2714–2723
28. Watanabe Y, Nakajima K, Shimamori Y, Fujimoto Y (1997) Biochem Mol Med 61:47–51
29. Manzetti S, Barnard R (2001) Combined Conference Abstracts, COMBIO2001, Pos-2-018
30. Brinkworth RI, Horne J, Kobe B (2002) J Mol Recognit 15:104–111
31. Lavigne P, Bagu JR, Boyko R, Willard L, Holmes CF, Sykes BD (2000) Protein Sci 9:252-264
32. Ferguson D (1995) J Comput Chem 16:501–511
33. Lindahl E, Hess B, van der Spoel D (2001) J Mol Mod 7:306–317
34. Kaminski GA, Friesner RA, Tirado-Rives J, Jorgensen WL (2000) OPLS-AA/L force field for proteins: Using accurate quantum mechanical data. Schrödinger Inc, at the 220th ACS National Meeting August 20–24, 2000, Washington D.C.
35. Berendsen HJC, Postma JPM, van Gunsteren WF, Hermans J (1981) Interaction models for water in relation to protein hydration. In: Reidel D, Pullman B (eds) Intermolecular forces. Publishing Company Dordrecht, pp 331–342
36. Schreiber H, Steinhauser O (1992) J Mol Biol 228:909–923
37. Berendsen HJC, Postma JPM, DiNola A, Haak JR (1984) J Chem Phys 81:3684–3690
38. Hess B, Bekker H, Berendsen HJC, Fraaje JGEM (1997) J Comp Chem 18:1463–1472
39. Alberts J, Nadassy K, Wodak SJ (1998) Protein Sci 7:1700–1716
40. Humphrey W, Dalke A, Schulten K (1996) J Mol Graphics 14:33–38
41. Dhanaraj V, Ye QZ, Johnson LL, Hupe DJ, Ortwine DF, Dunbar JB, Rubin JR, Pavlovsky A, Humblet C, Blundell TL (1996) Structure 4:375–386
42. Dhanaraj V, Ye QZ, Johnson LL, Hupe DJ, Ortwine DF, Dunbar JB Jr, Rubin JR, Pavlovsky A, Humblet C, Blundell TL (1996) Drug Des Discov 13:3–14
43. Gall AL, Ruff M, Kannan R, Cuniasse P, Yiotakis A, Dive V, Rio MC, Basset P, Moras D (2001) J Mol Biol 307:577–586
44. Rose C, Voisin S, Gros C, Schwartz JC, Ouimet T (2002) Biochem J 363:697–705
45. Tyndall JD, Fairlie DP (2001) Curr Med Chem 8:893–907
46. Glenn MP, Pattenden LK, Reid RC, Tyssen DP, Tyndall JD, Birch CJ, Fairlie DP (2001) J Med Chem 45:371–381
47. White SH, Wimley WC (1998) Biochim Biophys Acta 1376:339–352
48. Maskos K, Fernandez-Catalan C, Huber R, Bourenkov GP, Bartunik H, Ellestad GA, Reddy P, Wolfson MF, Rauch CT, Castner BJ, Davis R, Clarke HR, Petersen M, Fitzner JN, Cerretti DP, March CJ, Paxton RJ, Black RA, Bode W (1998) Proc Nat Acad Sci USA 95:3408–3412